Collective Dynamics in Liquid Aluminum near the Melting Temperature: Theory and Computer Simulation

A. V. Mokshin[a,b,*], R. M. Yulmetyev[a,b], R. M. Khusnutdinov[a,b], and P. Hänggi[c]

[a] *Kazan State University, Kremlevskaya ul. 18, Kazan, 420008 Tatarstan, Russia*

[b] *Kazan State Pedagogical University, Kazan, 420021 Russia*

* *e-mail: mav@theory.kazan-spu.ru*

[c] *University of Augsburg, Augsburg, D-86135 Germany*

Abstract—The microscopic collective dynamics of liquid aluminum near the melting temperature has been studied using two independent methods: first, using a theoretical approach developed in terms of the Zwanzig–Mori formalism and based on Bogolyubov's idea of reduced description of relaxation processes in liquids; second, using molecular dynamics simulation. The X-ray inelastic scattering spectra obtained with the theoretical approach and computer simulation are compared with experimental data. The high-frequency acoustic excitations that appear on microscopic spatial scales in liquid aluminum are found to be mainly caused by two-, three-, and four-particle interactions.

1. INTRODUCTION

Studying dynamic processes and transport phenomena in disordered systems is one of the most important problems of the modern physics of condensed matter [1, 2]. For example, the collective dynamics of particles on spatial scales of the order of several interatomic distances in liquids has currently aroused particular interest [3]. This is related in part to the improvement of experimental technique intended for inelastic neutron scattering, to the appearance of the third-generation sources of synchrotron radiation, and to the development of the technique of inelastic X-ray scattering (where the response is strictly coherent and the dynamic structure factor $S(k, \omega)$ is directly measured) [3, 4].

Numerous experimental studies have found that the frequency spectra of the dynamic structure factors of liquid metals have a three-peak shape even outside the hydrodynamic (microscopic) spatial region, where one elastic ($\omega = 0$) and two inelastic ($\omega_c \neq 0$) peaks exist, just as in the hydrodynamic Rayleigh–Mandelshtam–Brillouin triplet. The latter two peaks indicate the appearance of collective excitations. As the wavevector k increases, the high-frequency collective excitation frequency $\omega_c(k)$ increases, reaches its maximum at $k_m/2$ (where k_m is the position of the main maximum in the static structure factor $S(k)$), and then decreases. When the so-called de Genes narrowing zone is approached, the high-frequency peaks disappear.

The presence of high-frequency collective excitations in liquid aluminum at finite wavevectors has experimentally been revealed only recently [3, 5]. This result is supported (mostly qualitatively) by molecular dynamics simulation using various models for interparticle interaction potentials. The microstructure and dynamics of liquid aluminum near the melting point were first studied by molecular dynamics simulation in [6], where the local Ashcroft pseudopotential [7] and two nonlocal pseudopotentials were used. Although the static characteristics calculated with all three potentials are in good agreement with experimental data, the simulated dynamic structure factor spectra differ from experimental data. The static characteristics and microscopic dynamics of liquid aluminum have recently been studied by ab initio molecular dynamics simulation using the orbital-free (OF-AIMD) [8] and Kohn–Sham (KS-AIMD) [9] methods. In particular, the dynamic structure factor $S(k, \omega)$ was calculated and compared with experimental data on inelastic X-ray scattering [5]. Although the calculation results also exhibit a three-peak shape of $S(k, \omega)$, the heights and positions of the side peaks differ significantly from the experimental values.

Several theoretical approaches were proposed to explain the triplet structure of $S(k, \omega)$ in liquid aluminum at finite wavevectors: for example, a semiempirical modified hydrodynamic model [6, 10] or an approach based on a generalized Langevin equation and the viscoelastic model of [5]. These theories repro-

duce certain specific features of experimental $S(k, \omega)$ spectra. Nevertheless, they have the following disadvantages: the time dependences of relaxation processes are approximated using simplified model functions, and they introduce various fitting parameters.

In this work, we describe microscopic dynamics in liquid aluminum with another theoretical approach; it is based on the Zwanzig–Mori formalism and ideas concerning reduced description of relaxation processes [11]. It should be noted that a similar approach has been successfully applied earlier to describe the microscopic dynamics of particles in liquid alkali metals [12–15]. We also performed molecular dynamics simulations using the "glue" interparticle potential proposed in [16, 17]. The frequency spectra of the scattering intensity in liquid aluminum calculated by the two methods were compared with experimental data.

2. THEORETICAL FORMALISM

The intensity of inelastic X-ray scattering $I(k, \omega)$ in the system under study is connected with the dynamic structure factor $S(k, \omega)$ by the relation [3, 4, 18]

$$I(k, \omega) = \int \frac{\hbar\beta\omega'}{1 - e^{-\hbar\beta\omega'}} R(k, \omega - \omega') S(k, \omega') d\omega, \quad (1)$$

where $\beta = 1/k_B T$; k_B and T are the Boltzmann constant and the system temperature, respectively; $R(k, \omega)$ is the experimental resolution function; and the dynamic structure factor $S(k, \omega)$ contains detailed information on the collective properties of the system. As was shown in famous work [19], the $S(k, \omega)$ spectrum is connected with the autocorrelation function of local-density fluctuations

$$\phi(k, t) = \frac{\langle \rho^*(k, 0)\rho(k, t)\rangle}{\langle |\rho(k, 0)|^2\rangle} \quad (2)$$

through its Laplace transform

$$\tilde{\phi}(k, z) = \int_0^\infty e^{-zt}\phi(k, t) dt$$

by the relation

$$S(k, \omega) = \frac{S(k)}{\pi} \mathrm{Re}[\tilde{\phi}(k, z = i\omega)]. \quad (3)$$

Here,

$$S(k) = \langle |\rho(k, t)|^2\rangle$$

is the static structure factor of the liquid,

$$S(k) = 1 + \frac{Nm}{V}\int \exp(i\mathbf{k}\cdot\mathbf{r})[g(r) - 1] dr, \quad (4)$$

where V is the system volume, $g(r)$ is the radial pair distribution function, and the angle brackets $\langle \ldots \rangle$ indicate ensemble averaging. Thus, to determine the dynamic structure factor and the scattering intensity, we have to know the time behavior of the autocorrelator of local-density fluctuations $\phi(k, t)$ or its frequency spectrum.

We now consider an isotropic system consisting of N particles of mass m. The initial dynamic variable is taken to be the local-density fluctuations of the number of particles

$$\rho(\mathbf{k}, t) = \frac{1}{\sqrt{N}} \sum_{j=1}^{N} \exp(i\mathbf{k}\cdot\mathbf{r}_j(t)), \quad (5)$$

whose time evolution is specified by the equation of motion

$$\frac{d\rho(\mathbf{k}, t)}{dt} = i\hat{\mathcal{L}}\rho(\mathbf{k}, t), \quad (6)$$

where $\hat{\mathcal{L}}$ is the Liouville operator,

$$\hat{\mathcal{L}} = -i\sum_j \frac{\mathbf{p}_j}{m}\cdot\frac{\partial}{\partial\mathbf{r}_j} - i\sum_j \mathbf{F}_j\frac{\partial}{\partial\mathbf{p}_j}, \quad (7)$$

and $\mathbf{F}_j$ is the total force acting on the jth particle.

Using the Gram–Schmidt orthogonalization, we then obtain an infinite set of orthogonal dynamic variables

$$\begin{gathered}\mathbf{A}(k) = \{A_0(k), A_1(k), A_2(k), \ldots, A_j(k), \ldots\},\\ k = |\mathbf{k}|,\\ \langle A_j^* A_l\rangle = \delta_{j,l}\langle |A_j|^2\rangle,\\ A_0(k) \equiv \rho(k),\end{gathered} \quad (8)$$

they are connected by the recurrent relations

$$\begin{gathered}A_{j+1}(k) = i\hat{\mathcal{L}}A_j(k) + \Omega_j^2(k)A_{j-1}(k),\\ j = 0, 1, 2, \ldots, \quad A_{-1} \equiv 0,\end{gathered} \quad (9)$$

where $\delta_{j,l}$ is the Kronecker delta and

$$\Omega_j^2(k) = \frac{\langle |A_{j+1}(k)|^2\rangle}{\langle |A_j(k)|^2\rangle} \quad (10)$$

is the frequency relaxation parameter of the jth order having the dimensions of frequency squared.

By analogy with Eq. (2), we define the time autocorrelation functions of the dynamic variables $A_j(k)$ as follows:

$$M_j(k,t) = \frac{\langle A_j^*(k,0)A_j(k,t)\rangle}{\langle |A_j(k,0)|^2\rangle}, \qquad M_0(k,t) \equiv \phi(k,t), \tag{11}$$

they have the properties

$$\lim_{t\to 0} M_j(k,t) = 1, \tag{12}$$

$$0 \le |M_j(k,t)| \le 1, \tag{13}$$

$$\lim_{t\to\infty} M_j(k,t) = 0. \tag{14}$$

Property (12) follows directly from definition (11); the limit in Eq. (14) is valid for ergodic processes and results from the principle of long-term correlation weakening; and Eq. (13) can easily be derived from well-known Schwartz's inequality [20]. It should be noted that, if $M_0(k, t) = \phi(k, t)$ specifies local-density autocorrelations, then the $M_1(k, t)$ function corresponds to the time autocorrelation function of longitudinal momentum component fluctuations, $M_2(k, t)$ is directly related to the time autocorrelation function of energy fluctuations, and so on. In other words, at $k \longrightarrow 0$, the values of $M_0(k, t)$, $M_1(k, t)$, and $M_2(k, t)$ can be compared with the time autocorrelation functions corresponding to three retained hydrodynamic variables.

We now determine the normalized frequency moments of the dynamic structure factor:

$$\omega^{(2p)}(k) = \frac{\int_{-\infty}^{\infty} \omega^{2p} S(k,\omega)d\omega}{\int_{-\infty}^{\infty} S(k,\omega)d\omega} = (-i)^p \frac{d^p\phi(k,t)}{dt^p}\bigg|_{t=0}, \qquad p = 1, 2, \ldots. \tag{15}$$

It should be noted that only even moments ($p = 2, 4, \ldots$) take finite values and that odd moments become zero. Taking into account the second equality in the last equation, we can represent the short-term behavior of the $\phi(k, t)$ function in the form of the Taylor series

$$\phi(k,t) = 1 - \frac{1}{2!}\omega^{(2)}(k)t^2 + \frac{1}{4!}\omega^{(4)}(k)t^4 - \frac{1}{6!}\omega^{(6)}(k)t^6 + \ldots. \tag{16}$$

By making allowance for the relation

$$i^{(2j)}\frac{d^{2j}\phi(t)}{dt^{2j}}\bigg|_{t=0} = \frac{\langle [(i\hat{\mathcal{L}}A_0)^j]^*(i\hat{\mathcal{L}}A_0)^j\rangle}{\langle |A_0|^2\rangle}, \tag{17}$$

which holds true at a fixed k, we can obtain the following useful expressions relating the frequency moments $\omega^{(2j)}(k)$ to the frequency parameters $\Omega_j^2(k)$ from Eqs. (9) and (10):

$$\Omega_1^2(k) = \omega^{(2)}(k),$$

$$\Omega_2^2(k) = \frac{\omega^{(4)}(k)}{\omega^{(2)}(k)} - \omega^{(2)}(k),$$

$$\Omega_3^2(k) = \frac{\omega^{(6)}(k)\omega^{(2)}(k) - (\omega^{(4)}(k))^2}{\omega^{(4)}(k)\omega^{(2)}(k) - (\omega^{(2)}(k))^3},$$

$$\Omega_4^2(k) = \frac{1}{\Omega_1^2(k)\Omega_2^2(k)\Omega_3^2(k)}\{\omega^{(8)}(k) - \Omega_1^2(k) \times [(\Omega_1^2(k) + \Omega_2^2(k))^3 + 2\Omega_2^2(k)\Omega_3^2(k)(\Omega_1^2(k) + \Omega_2^2(k)) + \Omega_2^2(k)\Omega_3^4(k)]\}. \tag{18}$$

From definition (10), we can readily derive expressions for the frequency parameters $\Omega_j^2(k)$. For example, for the first three parameters $\Omega_1^2(k)$, $\Omega_2^2(k)$, and $\Omega_3^2(k)$, we have

$$\Omega_1^2(k) = \frac{k_BT}{m}\frac{k^2}{S(k)}, \tag{19}$$

$$\Omega_2^2(k) = 3\frac{k_BT}{m}k^2 + \frac{\rho}{m}\int \nabla_l^2 u(r)[1 - \exp(i\mathbf{k}\cdot\mathbf{r})]g(r)d^3r - \Omega_1^2(k), \tag{20}$$

$$\Omega_3^2(k) = \frac{15}{\Delta_2(k)}\left(\frac{k_BT}{m}k^2\right)^2 - \frac{[\Omega_1^2(k) + \Omega_2^2(k)]^2}{\Omega_2^2(k)} + \frac{\mathcal{U}(k)}{\Omega_1^2(k)\Omega_2^2(k)}, \tag{21}$$

where $\mathcal{U}(k)$ is a combination of integral expressions containing the interparticle interaction potential $u(r)$ and the three-particle distribution function $g_3(\mathbf{r}, \mathbf{r}')$. A complete expression for $\mathcal{U}(k)$ is given in [21]. Note that, as order j increases, the expressions for the fre-

Table 1. Frequency relaxation parameters Ω_j^2 ($\times 10^{26}$ s^{-2}) obtained from experimental data on inelastic X-ray scattering [5]

k, nm^{-1}	$\Omega_1^2(k)$	$\Omega_2^2(k)$	$\Omega_3^2(k)$	$\Omega_4^2(k)$	$\Omega_5^2(k)$	$\Omega_6^2(k)$
4.2	5.432	7.808	26.061	127.08	106.38	102.74
5.4	6.904	11.108	35.045	125.02	106.22	102.69
7.8	11.692	19.621	40.493	124.17	105.98	102.61
9.0	12.445	22.407	43.009	123.86	105.85	102.58

quency relaxation parameters $\Omega_j^2(k)$ become much more complex and begin to contain the equilibrium distribution functions of a group of j particles.

The authors of [22, 23] used the technique of projection operators and showed that the $\phi(k, t)$, $M_1(k, t)$, $M_2(k, t)$, … functions are connected by a chain of the integro-differential equations

$$\begin{aligned}
\frac{d\phi(k,t)}{dt} &= -\Omega_1^2(k)\int_0^t d\tau M_1(k,t-\tau)\phi(k,\tau),\\
\frac{dM_1(k,t)}{dt} &= -\Omega_2^2(k)\int_0^t d\tau M_2(k,t-\tau)M_1(k,\tau),\\
&\cdots\\
\frac{dM_j(k,t)}{dt} &= -\Omega_{j+1}^2(k)\int_0^t d\tau M_{j+1}(k,t-\tau)M_j(k,\tau),\\
& j = 1, 2, 3, \ldots.
\end{aligned} \tag{22}$$

With the Laplace transform, chain (22) can be written as the recurrent relation

$$\begin{aligned}
\tilde{M}_j(k,z) &= \frac{1}{z+\Omega_{j+1}^2(k)\tilde{M}_{j+1}(k,z)},\\
& j = 1, 2, 3, \ldots,
\end{aligned} \tag{23}$$

or the continued fraction

$$\begin{aligned}
\tilde{\phi}(k,z) &= \frac{1}{z+\Omega_1^2(k)\tilde{M}_1(k,z)}\\
&= \cfrac{1}{z+\cfrac{\Omega_1^2(k)}{z+\cfrac{\Omega_2^2(k)}{z+\cfrac{\Omega_3^2(k)}{z+\ldots}}}}.
\end{aligned} \tag{24}$$

The same result was obtained by the method of recurrent relations [18], which differs from the technique of projection operators. Note that, in both methods, Eq. (22) and, correspondingly, fraction (24) can exactly be derived from equation of motion (6).

Thus, the problem of finding $\phi(k, t)$ (or $\tilde{\phi}(k, z)$) can be reduced to the calculation of a certain time correlation function of the jth order $M_j(k, t)$, which eventually corresponds to the disconnection of the infinite chain of kinetic integro-differential equations (22) (i.e., to the break of fraction (24)). Another possible way is to calculate the frequency parameters $\Omega_j^2(k)$ appearing in fraction (24). The chain of Eqs. (22) can be disconnected by the following methods:

(i) the transition to the Markovian limit of Van Hove at a certain jth relaxation level, which is performed by introducing the so-called slow time $\tau = \lambda^2 t$ ($\lambda \longrightarrow 0$) [24];

(ii) the method of model memory functions, where the $M_j(k, t)$ function of the jth order is approximated by a certain simplified model function, such as an exponential function, a Gaussian function, or a hyperbolic secant or by their linear combination [25–29];

(iii) the mode-coupling approach [30], where the second-order memory function $M_2(k, t)$ is approximated by a polynomial of the initial time correlation function $\phi(k, t)$.

However, all these methods are approximate. Moreover, they contain a large number of fitting parameters having no clear physical meaning. In addition, it is difficult to directly determine the frequency parameters $\Omega_j^2(k)$ from Eqs. (19)–(21), since one has to calculate integral expressions containing distribution functions of many particles.

In this work, we propose another method to determine $\tilde{\phi}(k, z)$. As is seen from Eqs. (18), the frequency parameters $\Omega_j^2(k)$ can be derived from the frequency moments $\omega^{(j)}(k)$, which, in turn, can be obtained from experimental data on scattering. For example, using the data on the X-ray scattering intensity $I(k, \omega)$ in liquid aluminum at $T = 973$ K, we deconvolved Eq. (1) and found the frequency spectra of the dynamic structure factor $S(k, \omega)$ of the system under study at various wavevectors k, at which the frequency moments $\omega^{(j)}(k)$ were determined by Eqs. (15) and, then, the frequency parameters $\Omega_j^2(k)$ were determined. The calculated values of the first six frequency parameters are given in Table 1. It is obvious that the frequency parameters (just as the frequency moments) are very sensitive to the shape of the dynamic structure factor $S(k, \omega)$, whose experimental values contain certain errors. Moreover, as order j increases, the errors of the frequency parameters $\Omega_j^2(k)$ also increase. However, in the course of

calculations, we found that the ratios of the neighboring frequency parameters,

$$\xi_{j+1,j}(k) = \Omega^2_{j+1}(k)/\Omega^2_j(k),$$

are less sensitive to the from of $S(k, \omega)$. The values of $\xi_{j+1,j}(k)$ at the same wavevectors are given in Table 2.

As is seen from Tables 1 and 2, the first frequency parameters $\Omega^2_j(k)$ ($j = 1, 2, 3, 4$) increase with subscript j for all wavevectors, i.e., $\xi_{j+1,j}(k) > 1$ at $j = 1, 2, 3, 4$, whereas the frequency parameters of the fifth and sixth orders $\Omega^2_5(k)$ and $\Omega^2_6(k)$ are somewhat underestimated as compared to $\Omega^2_4(k)$. However, their ratios $\xi_{5,4}(k)$ and $\xi_{5,6}(k)$ are close to unity. Therefore, we may assume that

$$\Omega^2_4(k) = \Omega^2_5(k) = \Omega^2_6(k) = \ldots = \Omega^2_j(k), \quad j \geq 4. \tag{25}$$

In other words, beginning from $\Omega^2_4(k)$, the high-order frequency parameters virtually coincide.

From a physical viewpoint, this assumption means the following. Since the quantities reciprocal to the frequency parameters, i.e., $1/\Omega^2_j(k)$, characterize the quadratic time scales of the relaxation processes related to the fluxes of the $A_{j-1}(k)$ variables [2, 31], condition (25) allows us to pass from the infinite set of dynamic variables (9) to the finite set

$$\mathbf{A}(k) = \{A_0(k), A_1(k), A_2(k), A_3(k), A_4(k)\}, \tag{26}$$

that is, it allows us to decrease the number of variables required for the description of the collective dynamics of particles [11]. As was shown above, the autocorrelation functions of the variables from set (26) are related to the autocorrelators of the longitudinal components of the hydrodynamic variables and their fluxes.

With condition (25), we can also disconnect chain (22). To this end, we rewrite fraction (24) by making allowance for Eq. (25):

$$\tilde{M}_3(k, z) = \cfrac{1}{z + \cfrac{\Omega^2_4(k)}{z + \cfrac{\Omega^2_4(k)}{z + \cfrac{\Omega^2_4(k)}{z + \ldots}}}}. \tag{27}$$

As is known from the theory of continued fractions [32], a fraction of type (27) corresponds to the function (in the variable z)

$$\tilde{M}_3(k, z) = \frac{-z + [z^2 + 4\Omega^2_4(k)]^{1/2}}{2\Omega^2_4(k)}. \tag{28}$$

By applying the inverse Laplace transform to Eq. (28), we obtain

$$M_3(k, t) = \frac{1}{\sqrt{\Omega^2_4(k)}t} J_1(2\sqrt{\Omega^2_4(k)}t), \tag{29}$$

where J_1 is the first-order Bessel function. Substituting Eq. (28) into fraction (24), we obtain $\tilde{\phi}(k, z)$ and, making allowance for Eq. (3), find the following expression for the dynamic structure factor:

$$\begin{aligned} S(k, \omega) = {} & \frac{S(k)}{2\pi}\Omega^2_1(k)\Omega^2_2(k)\Omega^2_3(k)[4\Omega^2_4(k) - \omega^2]^{1/2} \\ & \times \{\Omega^4_1(k)\Omega^4_3(k) + \omega^2[\Omega^4_1(k)\Omega^2_4(k) - 2\Omega^2_1(k)\Omega^4_3(k) \\ & - \Omega^4_1(k)\Omega^2_3(k) + 2\Omega^2_1(k)\Omega^2_2(k)\Omega^2_4(k) \\ & + \Omega^4_2(k)\Omega^2_4(k) - \Omega^2_1(k)\Omega^2_2(k)\Omega^2_3(k)] \\ & + \omega^4[\Omega^4_3(k) - 2\Omega^2_1(k)\Omega^2_4(k) + 2\Omega^2_1(k)\Omega^2_3(k) \\ & - 2\Omega^2_2(k)\Omega^2_4(k) + \Omega^2_2(k)\Omega^2_3] \\ & + \omega^6[\Omega^2_4(k) - \Omega^2_3(k)]\}^{-1}. \end{aligned} \tag{30}$$

Table 2. Ratios of the neighboring frequency relaxation parameters $\xi_{j+1,j}(k) = \Omega^2_{j+1}(k)/\Omega^2_j(k)$, where $j = 1, 2, 3, 4$, and 5

k, nm^{-1}	$\xi_{2,1}$	$\xi_{3,2}$	$\xi_{4,3}$	$\xi_{5,4}$	$\xi_{6,5}$
4.2	1.4373	3.3377	4.8763	0.8371	0.9658
5.4	1.6087	3.1549	3.5674	0.8496	0.9668
7.8	1.6782	2.0638	3.0665	0.8535	0.9682
9.0	1.8005	1.9194	2.8799	0.8546	0.9691

3. COMPUTER DYNAMICS SIMULATION AND ITS DETAILS

Atomic dynamics can also be studied with computer simulation. We investigated the thermodynamic state of liquid aluminum having a numerical density $n = 0.052763$ Å^{-3} (mass density $\rho_\mu = 2.36$ g/cm^3) and a temperature $T = 1000$ K (melting temperature $T_m = 933.47$ K). We consider a system of $N = 4000$ particles

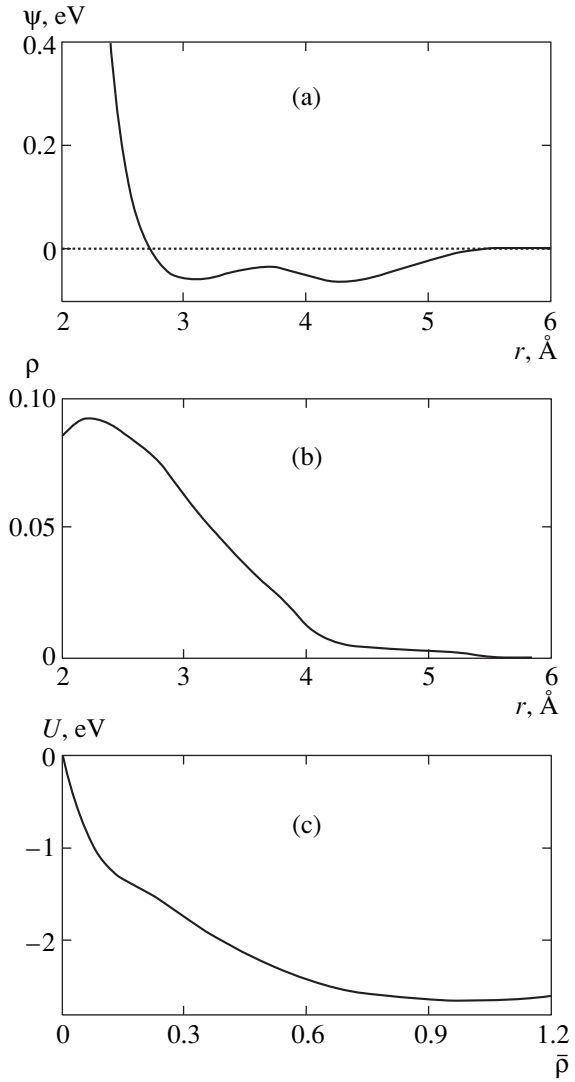

Fig. 1. (a) $\psi(r)$, (b) $\rho(r)$, and (c) $U(\bar{\rho})$ functions determining the interparticle interaction potential [16, 17] for liquid aluminum.

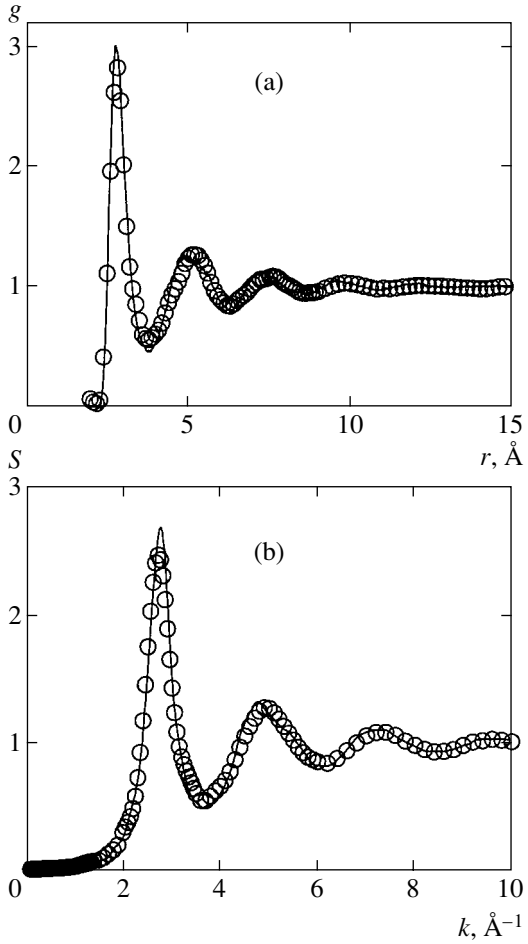

Fig. 2. (a) Radial distribution function $g(r)$ and (b) the static structure factor $S(k)$ for liquid aluminum: (solid line) molecular dynamics simulation at $T = 1000$ K and a mass density $\rho_\mu = 2.36$ g/cm^3 and (symbols) experimental data on X-ray scattering at $T = 943$ K [34, 35].

in a cubic cell ($L = 42.32$ Å) with periodic boundary conditions. Particles interact through the so-called glue potential [16, 17]

$$E = E_{\text{pair}} + E_{\text{glue}} = \sum_{i<j} \psi(r_{ij}) + \sum_i U(\bar{\rho}_i), \qquad (31)$$

which contains a short-range pair potential $\psi(r)$, a multiparticle glue function $U(\bar{\rho})$, and a $\bar{\rho}_i$ function. The latter is defined as

$$\bar{\rho}_i = \sum_j \rho(r_{ij}), \qquad (32)$$

where $\rho(r)$ is the atomic density. The $\psi(r)$, $\rho(r)$, and $U(\bar{\rho})$ functions are shown in Fig. 1. To reduce the calculation time, we neglected particle interaction at a distance $r \geq r_c$, where $r_c = 5.558$ Å is the cutoff radius.

The initial conditions were taken to be a particle configuration corresponding to the face-centered cubic lattice of crystalline aluminum with a lattice parameter $a = 4.23$ Å. To integrate the equation of motion, we used the Verlet algorithm with time step $\Delta t = 10^{-14}$ s [33]. 15000 time steps were executed to bring the system to an equilibrium state, and 100000 time steps were executed to average the time correlation functions. The average equilibrium characteristics and time correlation functions were obtained by averaging over the number of particles and time.

4. COMPARISON WITH EXPERIMENT AND DISCUSSION OF THE RESULTS

Figure 2 shows the simulated radial distribution function $g(r)$ of liquid aluminum at $T = 1000$ K and the static structure factor $S(k)$ found from Eq. (4). Both

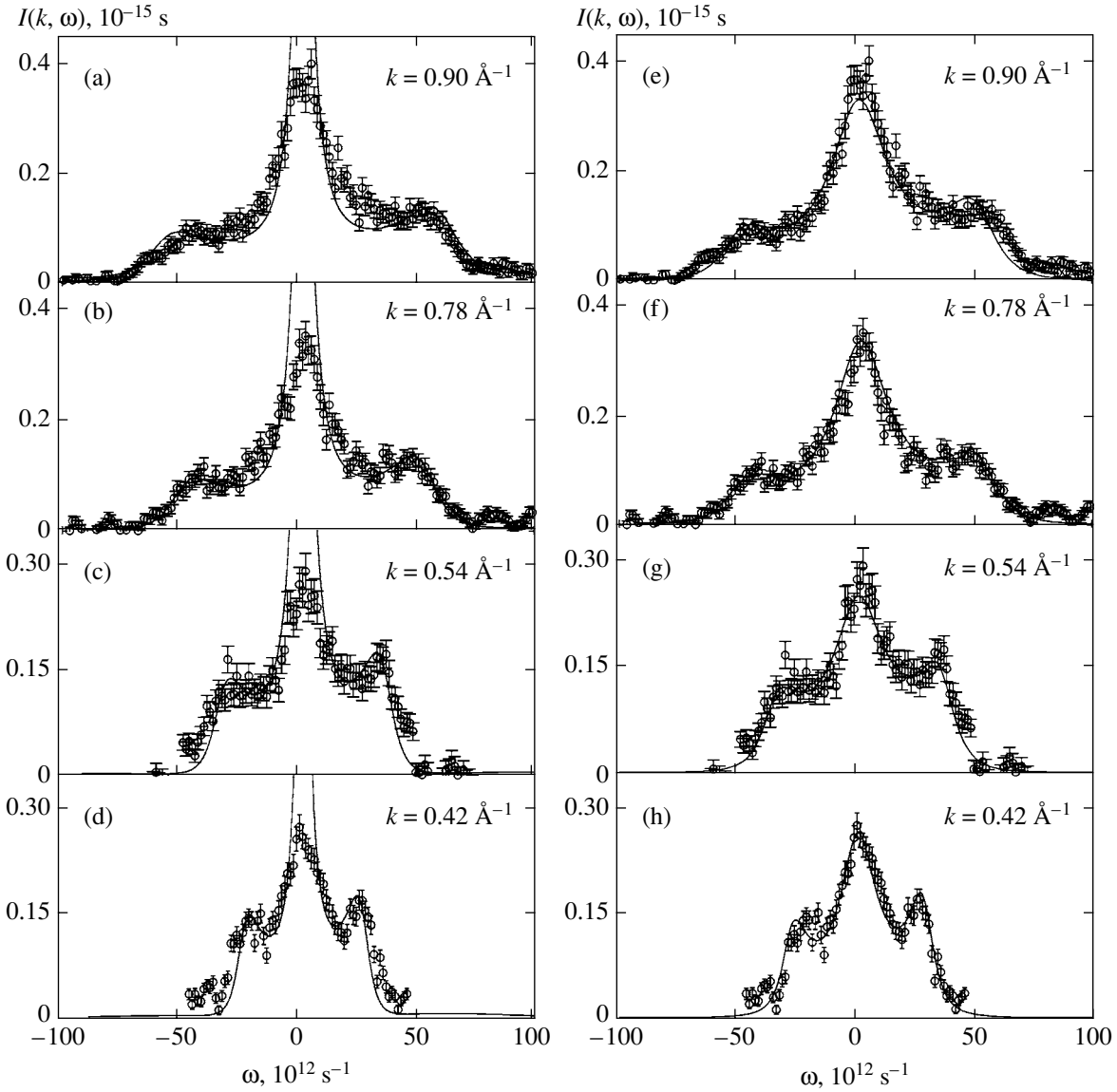

Fig. 3. Frequency spectra of the scattering intensity $I(k, \omega)$ in liquid aluminum at $T = 1000$ K at various wavevectors k: (a–d) solid line illustrates the molecular dynamics simulation and (e–h) solid line illustrates the results of theoretical model (30) for the corresponding wavevectors k. The experimental data on inelastic X-ray scattering [5] are shown by symbols.

functions are compared with experimental data on X-ray scattering [34, 35]. The simulation results are seen to reliably characterize the fine structure of the system under study and to exactly reproduce the experimental data. Therefore, it is interesting to test the chosen potential model to describe the nonequilibrium characteristics of the system. To this end, we used the simulation results to calculate the dynamic structure factor directly from definition (3) with autocorrelator (2) and the local density specified by Eq. (5). For comparison with the experimental data, we took into account the condition of detailed balance and the experimental resolution according to Eq. (1). The $I(k, \omega)$ results obtained are shown in Figs. 3a–3d. The glue-potential simulation results are seen to correctly reproduce the high-frequency portions of the experimental X-ray scattering spectra at all wavevectors k: they correctly predict the positions, heights, and decrease of the side peaks. However, the simulated height of the central peak (at $\omega = 0$) is slightly overestimated. This discrepancy can be caused by the fact that the time interval in the computer experiment is limited (finite).

The X-ray scattering intensity $I(k, \omega)$ in liquid aluminum was also calculated using theoretical model (30) developed for the dynamic structure factor. The frequency parameters $\Omega_1^2(k)$, $\Omega_2^2(k)$, $\Omega_3^2(k)$, and $\Omega_4^2(k)$ used for the calculations are given in Table 1, and the values of the static structure factor $S(k)$ are borrowed from [34, 35]. The calculated and experimental results

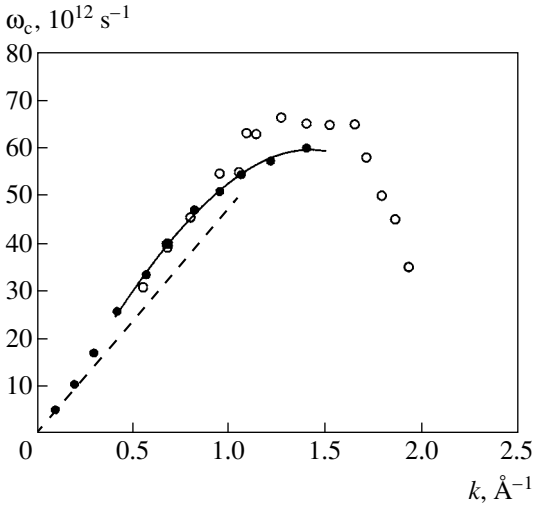

Fig. 4. Dispersion of the side ω_c peak: (filled circles) experimental data on inelastic X-ray scattering [5]; (open circles) molecular dynamics simulation; and (dashed line) extrapolated hydrodynamic result $\omega_c(k) = c_s k$, where c_s is the sound velocity.

are compared in Figs. 3e–3h. The calculated scattering intensity $I(k, \omega)$ spectra are seen to coincide with the experimental data of [5].

Figure 4 shows the dispersions of the high-frequency $I(k, \omega)$ peak determined from the experimental data, by the glue-potential simulation, and by the theoretical model developed. The theoretical values of $\omega_c(k)$ are seen to precisely reproduce the experimental results, whereas the simulation results are higher than the experimental values at wavevectors $k \geq 9$ nm^{-1}. Moreover, all (experimental, simulation, and theoretical) results indicate the presence of the so-called positive dispersion effect [2] in the microscopic region under study: the values of $\omega_c(k)$ exceed the values predicted by the usual hydrodynamic theory with a linear dispersion [36] and a sound velocity $c_s = 4750$ m/s [3, Table 1; 37].

As follows from an analysis of Eq. (30), the positions of $\omega_c(k)$ and the widths of the side peaks in the spectra of the dynamic structure factor $S(k, \omega)$ (and, correspondingly, the $I(k, \omega)$ intensities) are determined by the solutions of the bicubic polynomial in frequency ω in the denominator of Eq. (30). The coefficients of this polynomial are specified by the first four frequency parameters $\Omega_j^2(k)$ ($j = 1, 2, 3, 4$), whose values depend on the corresponding equilibrium j-particle equilibrium distributions. An important conclusion follows from these results: the high-frequency collective excitations that are observed on microscopic spatial scales in liquid aluminum as the side $I(k, \omega)$ peaks are mainly caused by two-, three-, and four-particle interactions.

5. CONCLUSIONS

We theoretically described the collective dynamics of particles that occurs on microscopic spatial scales in liquid aluminum near the melting temperature and showed that the idea of reduced description can be actualized using the experimentally observed equalization of the time scales of relaxation processes. In the case of liquid aluminum, this equalization of the time scales of high-order dynamic variables was detected by analyzing the latest experimental data on inelastic X-ray scattering. This equalization can be explained by the fact that, on spatial scales comparable with the interatomic distances, the role of fast relaxation processes (~10^{-14} s) becomes substantial and that the hydrodynamic variables cease to be slow as compared to other variables [2].

Screening effects also significantly affect ionic motion in liquid aluminum. Therefore, in the case of liquid aluminum, it is rather difficult to choose an appropriate model for an interparticle interaction potential, in contrast to liquid alkali metals (where ionic motion is accurately determined by pairwise screened ion–ion interactions). In this work, we showed that the glue potential used earlier for studying cluster formation [16, 17] can successfully be employed to describe both the structural properties of liquid aluminum and the collective dynamics of particles in it.

We also revealed that the high-frequency collective dynamics of this system is directly related to three- and four-particle interactions along with two-particle interactions. Our analysis indicates that the correlations of a large number of particles on these spatial scales turn out to be actually insignificant.

ACKNOWLEDGMENTS

We thank T. Scopigno for supplying the experimental data.

This work was supported by the Russian Foundation for Basic Research, project no. 05-02-16639.

REFERENCES

1. N. H. March, *Liquid Metals* (Cambridge Univ. Press, Cambridge, 1990).
2. U. Balucani and M. Zoppi, *Dynamics of the Liquid State* (Clarendon, Oxford, 1994).
3. T. Scopigno, G. Ruocco, and F. Sette, Rev. Mod. Phys. **77**, 881 (2005).
4. E. Burkel, *Inelastic Scattering of X-rays with Very High Energy Resolution* (Springer, Berlin, 1991).
5. T. Scopigno, U. Balucani, G. Ruocco, and F. Sette, Phys. Rev. E **63**, 011210 (2001).
6. I. Ebbsjö, T. Kinell, and I. Waller, J. Phys. C **13**, 1865 (1980).
7. N. W. Ashcroft, Phys. Lett. **23**, 48 (1966).
8. D. J. González, L. E. González, J. M. López, and M. J. Stott, Phys. Rev. B **65**, 184201 (2002).

9. M. M. G. Alemany, L. J. Gallego, and D. J. González, Phys. Rev. B **70**, 134206 (2004).
10. S. Singh and K. Tankeshwar, Phys. Rev. E **67**, 012201 (2003).
11. N. N. Bogolyubov, *Dynamical Problems in Statistical Physics* (Gostekhizdat, Moscow, 1946) [in Russian].
12. R. M. Yulmetyev, A. V. Mokshin, P. Hänggi, and V. Yu. Shurygin, Phys. Rev. E **64**, 057101 (2001).
13. R. M. Yulmetyev, A. V. Mokshin, P. Hänggi, and V. Yu. Shurygin, JETP Lett. **76**, 147 (2002).
14. R. M. Yulmetyev, A. V. Mokshin, T. Scopigno, and P. Hänggi, J. Phys.: Condens. Matter **15**, 2235 (2003).
15. A. V. Mokshin, R. M. Yulmetyev, and P. Hänggi, J. Chem. Phys. **121**, 7341 (2004).
16. F. Ercolessi, M. Parrinello, and E. Tosatti, Philos. Mag. A **58**, 213 (1988).
17. F. Ercolessi and J. B. Adams, Europhys. Lett. **26**, 583 (1994).
18. U. Balucani, M. H. Lee, and V. Tognetti, Phys. Rep. **373**, 409 (2003).
19. L. Van Hove, Phys. Rev. **95**, 249 (1954).
20. M. C. Reed and B. Simon, *Methods of Modern Mathematical Physics* (Academic, New York, 1972, Mir, Moscow, 1977).
21. E. Michler, H. Hahn, and P. Schofield, J. Phys. F: Met. Phys. **7**, 869 (1977).
22. R. Zwanzig, Phys. Rev. **124**, 1338 (1961).
23. H. Mori, Prog. Theor. Phys. **33**, 423 (1965); **34**, 399 (1965).
24. R. Zwanzig, Lect. Theor. Phys. **3**, 106 (1960).
25. N. K. Ailawadi, A. Rahman, and R. Zwanzig, Phys. Rev. A **4**, 1616 (1971).
26. R. Vogelsang and C. Hoheisel, Phys. Rev. A **35**, 1786 (1987).
27. K. Tankeshwar, G. S. Dubey, and K. N. Pathak, J. Phys. C: Solid State Phys. **21**, L811 (1988).
28. K. Tankeshwar, K. N. Pathak, and S. Ranganathan, J. Phys. Chem. Liq. **22**, 75 (1990).
29. M. J. Nuevo, J. J. Morales, and D. M. Heyes, Phys. Rev. E **55**, 4217 (1997).
30. W. Götze, in *Liquids, Freezing, and the Glass Transition*, Ed. by J. P. Hansen, D. Levesque, and J. Zinn-Justin (North-Holland, Amsterdam, 1991).
31. A. V. Mokshin, R. M. Yulmetyev, and P. Hänggi, Phys. Rev. Lett. **95**, 200601 (2005).
32. A. Ya. Khinchin, *Continued Fractions*, 4th ed. (Nauka, Moscow, 1978; Univ. Chicago Press, Chicago, 1964).
33. M. P. Allen and D. J. Tildesley, *Computer Simulation of Liquids* (Clarendon, Oxford, 1987).
34. Y. Waseda, *The Structure of Non-Crystalline Materials: Liquids and Amorphous Solids* (McGraw-Hill, New York, 1980).
35. IAMP database of SCM-LIQ (Tohoku Univ.), http://www.iamp.tohoku.ac.jp/database/scm.
36. L. D. Landau and E. M. Lifshitz, *Mechanics of Continuous Media,* 2nd ed. (Fizmatgiz, Moscow, 1959) [in Russian].
37. T. Iida and R. Guthrie, *The Physical Properties of Liquid Metals* (Oxford Sci., Oxford, 1993).

Translated by K. Shakhlevich